XMM-Newton CCF Release Note

XMM-CCF-REL-26

Effective area of the X-ray telescopes

P. Gondoin

October 5, 2000

1 CCF components

Name of CCF	VALDATE	List of Blocks changed	CAL VERSION	XSCS flag
XRT1_XAREAEF_0007	2000-01-13T00:00:00	ONAXISXAREAEF, VIGNETTING	Cal 3.80, xmm-sas_20000903_1900	NO
XRT2_XAREAEF_0008	2000-01-13T00:00:00	ONAXISXAREAEF, VIGNETTING	Cal 3.80, xmm-sas_20000903_1900	NO
XRT3_XAREAEF_0007	2000-01-13T00:00:00	ONAXISXAREAEF, VIGNETTING	Cal 3.80, xmm-sas_20000903_1900	NO

2 Changes

For technical reason, an artificial point was added at 0 eV in the on-axis effective area table.

3 Scientific Impact of this Update

This update has no impact on the on-axis effective area accuracy in the 100 eV to 20 keV band but is only provided for technical reasons.

4 Estimated Scientific Quality

The scientific quality of the refered CCF is identical to the previous release.

4.1 Numerical model accuracy

The in-orbit effective area of the CCF files were generated using scisim in combination with a numerical model of the x-ray telescopes [2]. The accuracy of the CCF files can be estimated by comparing on-ground calibration test measurements with simulation results [3]. Note however that on-ground calibration tests could not be performed in fully representative conditions. On-axis effective area (see Fig.1) were measured on mirror modules without x-ray baffles using sources located at a finite distance. The vignetting function of one telescope equipped with x-ray baffles was measured in a collimated beam in EUV at 58 nm (see Fig.2).

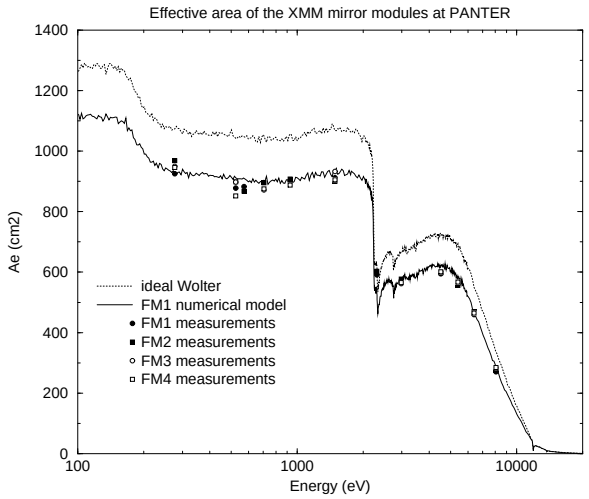

Figure 1: X-ray measurement and simulation of the on-axis effective area at PANTER

4.2 In-orbit calibration verification

The simulation results indicates calibration accuracy of the effective area on-axis better than 5 % over most of the XMM spectral range. A possible exception, however, is the gold M absorption edge due to the use of discrete spectral lines for effective area measurements on-ground.

Within the in-flight calibration programme, bright BL Lac objects with hard spectra were observed to obtain continuum emission spectra in the 2.2 to 3.4 keV range of the Au M absorption edges [4]. Their lineless continuum emission is well suited to map the edge discontinuities of the telescopes and instruments effective area. Fig.3 shows spectra of the MS1229.2+6430 BL Lac object obtained with the MOS cameras through thin Al filters. These spectra were fitted with single power law models plus a photo-electric absorption. The fit were performed using the XSPEC software package in combination with response matrix files identical for the two MOS cameras. These response files include effective area calibration files of the x-ray telescopes. No excess residuals to the fitting curve are observed around the 2.2 keV location of the Au M edge.

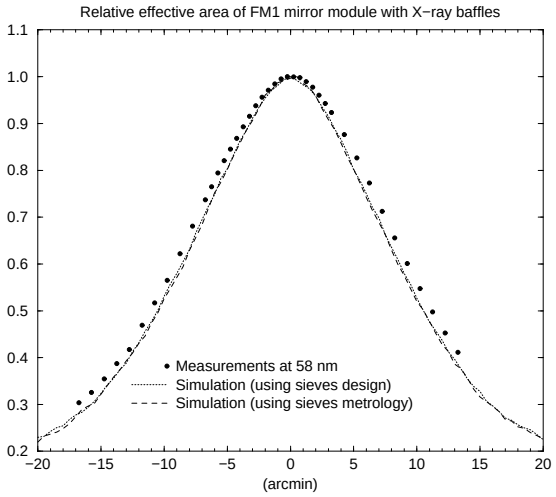

Figure 2: EUV measurement and simulation of the vignetting function at CSL

In order to verify the effective area variation over the EPIC field of view, the G21.5-0.9 supernova remnant was observed on-axis and at four off-axis positions [4, 5]. The 10 arcmin off-axis pointings in orthogonal direction were used in particular to verify the azimuthal variation of the vignetting function produced by the RGA assemblies. Indeed, the stack of gratings located behind the FM3 and FM4 telescopes acts as a Venitian blind. Due to the grating plane inclination with respect to the telescope optical axis, the vignetting function in the EPIC detector plane is modulated azimuthaly with the highest effective area in the RGA dispersion direction. Fig.4 show that the measurements confirm the azimuthal modulation of the vignetting function. At 10 arcmin off-axis angle, they are within 10% of the vignetting calculation using the present description of the RGA vignetting.

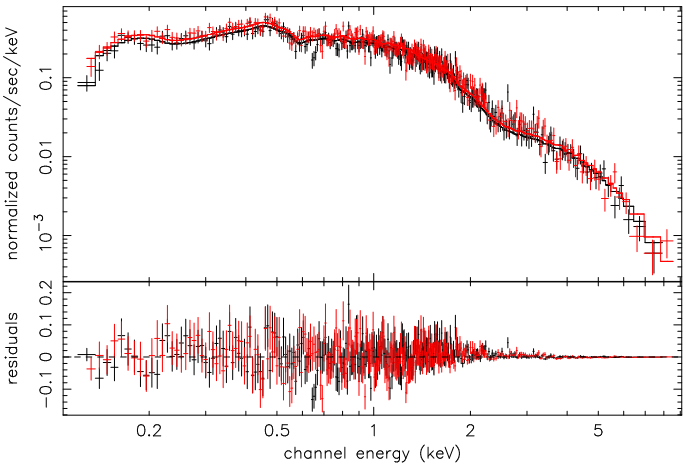

Figure 3: MOS 1 and 2 spectra of the MS1229.2+6430 BL Lac object including spectral fit residuals to a power law model with an absorbed column density.

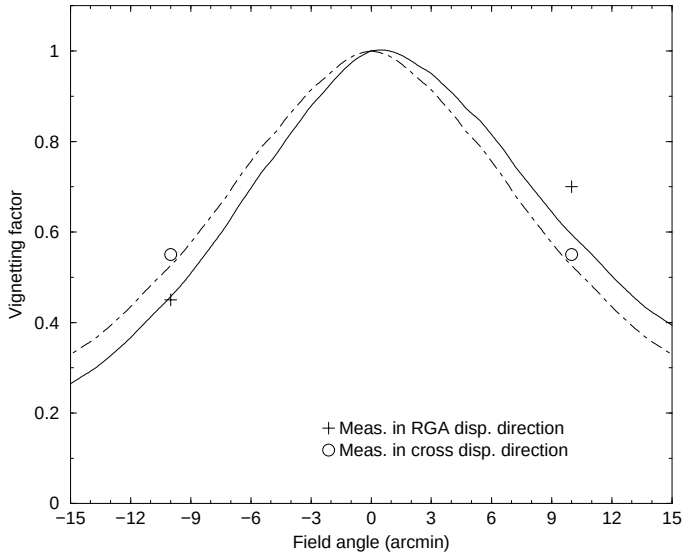

Figure 4: Angle dependance of the telescope plus RGA vignetting function below 4.5 keV in azimuth respectively parallel (continuous line) and perpendicular to the RGA dispersion.

References

[1] Christian Erd, Phillipe Gondoin, David Lumb, Rudi Much, Uwe Lammers, and Giuseppe Vacanti. *Calibration Access and Data Handbook*. XMM-PS-GM-20, issue 1.0, ESA/SSD, September 2000. http://xmm.vilspa.esa.es/calibration/docs/general/calhb.ps.gz.

[2] Ph. Gondoin, B. Aschenbach, H. Brauninger, D. de Chambure, J.P. Colette, R. Egger, K. van Katwijk, D. Lumb, A. Peacock, Y. Stockmann, J.P. Tock, and R. Willingale. *Simulation of the XMM Mirror Performance based on Metrology Data*. In *SPIE Proc.*, volume 2808, pages 390–401, 1996.

[3] Ph. Gondoin, B. Aschenbach, M. Beijersbergen, R. Egger, F. Jansen, Y. Stockman, and J.P. Tock. *Calibration of the first XMM flight mirror module: II. Effective Area*. In *SPIE Proc.*, volume 3444, page 290, 1998.

[4] Ph. Gondoin, B. Aschenbach, C. Erd, D.Lumb, S. Majerowicz, D. Neumann, and J.L.Sauvageot. *In-orbit calibration of the XMM-Newton telescopes*. In *SPIE Proc.*, 2000.

[5] D.M. Neumann. *Report of the in-flight vignetting calibration of the MOS cameras aboard the XMM-Newton satellite*. , CEA/Saclay, August 2000.